
EAP4EMSIG - ENHANCING EVENT-DRIVEN MICROSCOPY FOR MICROFLUIDIC SINGLE-CELL ANALYSIS

Nils Friederich^{1,2,*}, Angelo Jovin Yamachui Sitcheu^{1,*}, Annika Nassal^{1,2}, Erenus Yildiz³, Matthias Pesch⁴, Maximilian Beichter¹, Lukas Scholtes³, Bahar Akbaba¹, Thomas Lautenschlager¹, Oliver Neumann¹, Dietrich Kohlheyer⁴, Hanno Schar³, Johannes Seiffarth^{4,5,⊕}, Katharina Nöh^{4,⊕}, and Ralf Mikut^{1,⊕}

¹Institute for Automation and Applied Informatics (IAI), Karlsruhe Institute of Technology

²Institute of Biological and Chemical Systems (IBCS), Karlsruhe Institute of Technology

³Institute for Data Science and Machine Learning (IAS-8), Forschungszentrum Jülich GmbH

⁴Institute of Bio- and Geosciences (IBG-1), Forschungszentrum Jülich GmbH

⁵Computational Systems Biology (AVT-CSB), RWTH Aachen University

*Contributed Equally

⊕Supervised Equally

February 17, 2025

ABSTRACT

Microfluidic Live-Cell Imaging yields data on microbial cell factories. However, continuous acquisition is challenging as high-throughput experiments often lack realtime insights, delaying responses to stochastic events. We introduce three components in the Experiment Automation Pipeline for Event-Driven Microscopy to Smart Microfluidic Single-Cell Analysis: a fast, accurate Deep Learning autofocus method predicting the focus offset, an evaluation of real-time segmentation methods and a realtime data analysis dashboard. Our autofocus achieves a Mean Absolute Error of $0.0226\mu\text{m}$ with inference times below 50 ms. Among eleven Deep Learning segmentation methods, Cellpose 3 reached a Panoptic Quality of 93.58%, while a distance-based method is fastest (121 ms, Panoptic Quality 93.02%). All six Deep Learning Foundation Models were unsuitable for real-time segmentation.

1 Introduction

Microbes are ubiquitous, microscopic organisms that inhabit a wide range of environments—from extreme locations like hydrothermal vents to the human body, where they outnumber human cells by a factor of 1.3 [48, 1]. Their roles are critical in maintaining ecological balance by driving essential biogeochemical cycles such as the carbon, nitrogen, and sulfur cycles [28, 55]. Moreover, the human microbiome is indispensable for health, aiding in digestion, vitamin production, and immune defense, while industrial applications harness microbes for biotechnology, pharmaceuticals, and agriculture [26].

Given their importance, understanding microbial behavior, genetics, and interactions is key to advancements in biotechnology, environmental protection, and medical science. For instance, microbial research can lead to innovations such as the production of valuable compounds like insulin or biodegradable plastics [36] and support bioremediation efforts in oil spill and toxic waste cleanup [18].

Microfluidic Live-Cell Imaging (MLCI) enables a detailed exploration of the precise microbial growth dynamics at the single-cell level by generating large volumes of experimental data [41]. Accurate automated cell segmentation is essential to extract meaningful insights regarding growth behavior under various conditions. However, MLCI experiments typically involve the parallel cultivation of thousands of colonies rather than individual ones to gain robust quantitative insights. In these high-throughput experiments, a cell suspension is infused into a microfluidic device, where cells are randomly seeded into numerous growth chambers. Within each chamber, cells remain confined and

proliferate until the chamber is densely populated, often containing up to 1,000 cells. Manually analyzing such a vast number of colonies is not feasible due to the immense data volume and the labor-intensive nature of the task. Therefore, automated and intelligent processing, analysis, and experimental planning are indispensable.

Our work aims to overcome these technical barriers by proposing new methods and evaluations for three core components of Experiment Automation Pipeline for Event-Driven Microscopy to Smart Microfluidic Single-Cell Analysis (EAP4EMSIG), a tool designed to automate and intelligently manage MLCI experiments. Building on our previous work [15], we extend it in several important ways. First, we introduce a novel Machine Learning (ML)-based real-time autofocus module that improves information acquisition and enhances experimental efficiency. Second, we performed a comprehensive zero-shot evaluation on a microbe benchmark dataset [46] using 11 state-of-the-art pretrained segmentation models, including task-specific models, domain-specific models and Foundation Models (FMs), to identify the best-suited method in terms of real-time capability and accuracy. Finally, we present a new real-time data analysis dashboard to provide biology experts with detailed insights into ongoing experiments while offering enhanced control over experimental parameters.

2 Related Work

2.1 Autofocusing

Autofocusing is crucial for automated MLCI imaging, enabling sharp, clear images necessary for accurate data analysis. Traditional approaches are categorized as hardware-based and image-based. Hardware-based methods, such as dual-sensor scanning and beam splitter arrays, provide precise focus estimates, but they require expensive, complex equipment and are susceptible to the wear of mechanical components as well as the limitations of the microscope [5, 29]. In contrast, image-based methods rely on metrics such as sharpness or intensity variance, offering cost-effective solutions without additional hardware [54]. However, they often struggle with low-contrast samples, computational efficiency, and manual calibration requirements [49].

Recent advances in ML offer a promising alternative. Neural Network (NN) models can predict the optimal focus directly from image data, eliminating manual feature extraction and adapting to diverse imaging conditions [21, 30]. These methods, integrated into automation pipelines, enable real-time, human-independent adjustments [7]. Challenges remain, including the need for extensive annotated data and maintaining performance on novel organisms.

2.2 Real-time Image Segmentation

To analyze the microbial colonies in real-time experiments, a fast, accurate and precise segmentation is essential [32]. Classic methods [27, 37] are often unsuitable because they necessitate less accurate and time-consuming manual feature extraction [57]. Contrastingly, Deep Learning (DL)-based methods offer more automated, robust, accurate and faster segmentation [13]. The abundance of available data has significantly accelerated the development of advanced DL-based segmentation algorithms, resulting in a wide range of models [12]. The following are particularly noteworthy for biomedical image segmentation:

Task-specific models. Two methods developed especially for microbial image segmentation are of interest: first, the distance-based method [44, 47], which achieved impressive results in the Cell Tracking Challenge [34]; second, the Cellpose [52]-based Omnipose [8], designed for 2D & 2D+t, and 2D & 3D microbial data segmentation.

Domain-specific models. Recent advancements in biomedical image analysis have developed various image segmentation methods that generalize well across multiple tasks. Some notable models are: StarDist [45], Cellpose 3 [51] and Contour Proposal Network (CPN) [56].

Foundation models. The progress in self-supervised learning has facilitated the development of large-scale models that can segment various images across numerous tasks and domains. State-Of-The-Art (SOTA) models such as Segment Anything Model (SAM) [25], SAM 2 [42], SAM 2.1 [42], Florence-2 [58], BiomedParse [59] and 4M21 [3] are the most prominent and popular representees.

2.3 Experiment Automation Pipeline (EAP) Tools

Experiment automation in life science research combines laboratory hardware, software and biological components and has several advantages. For example, by reducing the variability caused by humans during experiments, reproducibility

can be genuinely improved [22]. However, due to the complexity of linking different components and the specificity of laboratory use cases, very few generic tools for experiment automation have been developed. Based on [15], Tab. 1 presents some EAP tools closely aligned to ours.

Despite the contribution of different tools towards experiment automation in life science, no tool provides a complete, modular, extendable and adaptable pipeline in the field of MLCI to the best of our knowledge.

Table 1: Overview of SOTA EAP methods based on the implemented modules along with their limitations regarding the context of this work. PYthon Microscopy Environment (PYME), Experiment Automation Pipeline for Dynamic Processes (EAPDP).

Method	Modules				Limitations
	Microscope control	Real-time image processing	Real-time data analysis	Real-time experiment planner	
CyberSco.Py [6]	✓	✓	✓	✓	Supports only U-Net
MicroMator [14]	✓	✓	✓	✓	Not actively used
Event-driven acquisition [33]	✓	✓	✓	✓	Other modules absent
Cheetah [38]	✓	✓	✓	✓	Supports only U-Net
Pycro-Manager [39]	✓	✓	✓		Other modules absent
Python-Microscope [40]	✓		✓		Other modules absent
PYME [4]	✓	✓	✓		Focus on super-resolution
EAPDP [17]	✓	✓	✓	✓	Focus on dynamic process modelling

3 Methodology

To automate microfluidic live-cell experiments, we proposed in [15] a new EAP approach that entails eight modules arranged in a cyclical process (see Fig. 1). The first module handles image acquisition, utilizing SOTA research microscope setups and low-cost 3D-printed microscope systems. Second, the real-time image processing is executed on incoming images, generating single-cell instance segmentation predictions. The generated data and metadata are saved and managed in an instance of the third module’s Open Microscopy Environment Remote Objects (OMERO) DataBase (DB) [2]. This instance also manages ground truth data generated with the cell simulator module CellSium [43] and the ObiWan-Microbi [47] semi-annotation module as the fourth and fifth modules. Sixth, the real-time data analysis module relies on recorded data to provide feedback via a dashboard and detect events. Based on these, the real-time experiment planner, as the seventh module, schedules the experiment continuously and sends the following steps to the microscope control module. This eighth module forwards these instructions back to the image acquisition module. In the following, we will focus on new methodological approaches to autofocus, real-time image processing and real-time data analysis.

3.1 Autofocusing

To address the challenge of autofocus, we propose a simplified, regression-based approach (see Fig. 2). We build a Multi-Layer Perceptron (MLP) NN with two hidden layers and train it on extracted features (Laplacian and Gaussian pyramids, wavelets and Log-Gabor filters) to predict the "focus offset"—the distance to the optimal focus frame within z-stacks, which is directly used by the microscope to approach the optimal focus. Augmentation techniques, including random flips and rotations, are used during training to improve robustness across various imaging conditions.

Using a step size of 0.1 μm , our method prioritizes achieving low Mean Absolute Error (MAE) while maintaining real-time prediction speeds and enabling fast and accurate focus adjustment without requiring extensive expert knowledge (see Fig. 2). The task is treated as a regression problem, predicting the "focus offset"—the distance to the optimal focus frame within z-stacks.

For model design, we prioritize simplicity and transparency by using a MLP rather than complex architectures like transformers.

3.2 Real-Time Image Processing

The image data acquired in the previous pipeline step is processed in the top left box in Fig. 1. First, the current chamber ID is detected using classical template matching [27] or DL-based methods such as You Only Look Once

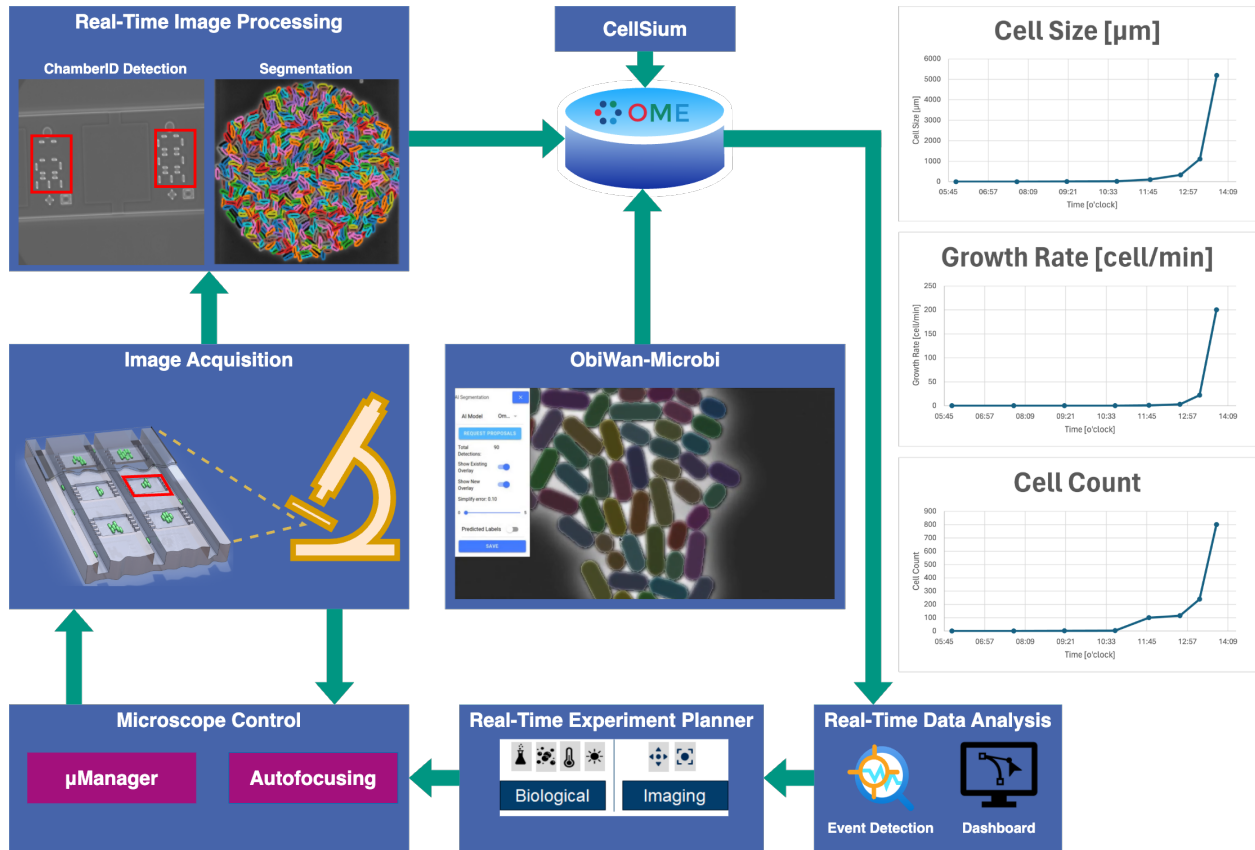


Figure 1: EAP4EMSIG visualization. The pipeline consists of eight modules, represented by the light blue boxes and the OMERO database, arranged in a cyclical process. The microbial images in the figure come from a dataset presented in [46]. The images from the experiment chip are from an internal dataset. Adapted from [15].

(YOLO) [23], which showed his strong performance in a wide range of contexts [10, 16, 53]. As the region of interest, the growth chamber needs to be extracted and any microfluidic structures must be removed from the images. Afterward, the content of the chamber is segmented using a suitable segmentation method. For our pipeline, we focused on SOTA DL segmentation methods (see Sec. 2.2), which are either task-specific models, domain-specific models or FMs and therefore allow us to address various segmentation tasks effectively. Regarding our target to create a live-cell experiment automation pipeline, real-time image processing is a key goal. Based on the microscope’s hardware, a processing time of less than 100 milliseconds is sufficient for this work. To find the most accurate DL method under these constrain, we did a benchmark to evaluate and compare the SOTA methods.

3.3 Real-Time Data Analysis

Upon real-time image processing, single-cell data such as cell mask, average cell size and growth rate are computed and saved. The real-time data analysis module leverages these data and metadata to provide insights into the ongoing experiment and help the human expert navigate the experiment. This module consists on the one hand of an event detection submodule that enables event-based experiment control and a dashboard on the other hand to visualize the acquired data. The dashboard combines a range of functionalities to support efficient monitoring and analysis of the experiment. Its modular architecture enables seamless integration of new features and capabilities without affecting the existing codebase, making it highly extendable and adaptable to other use cases. The dashboard is presented in Sec. 4.3.

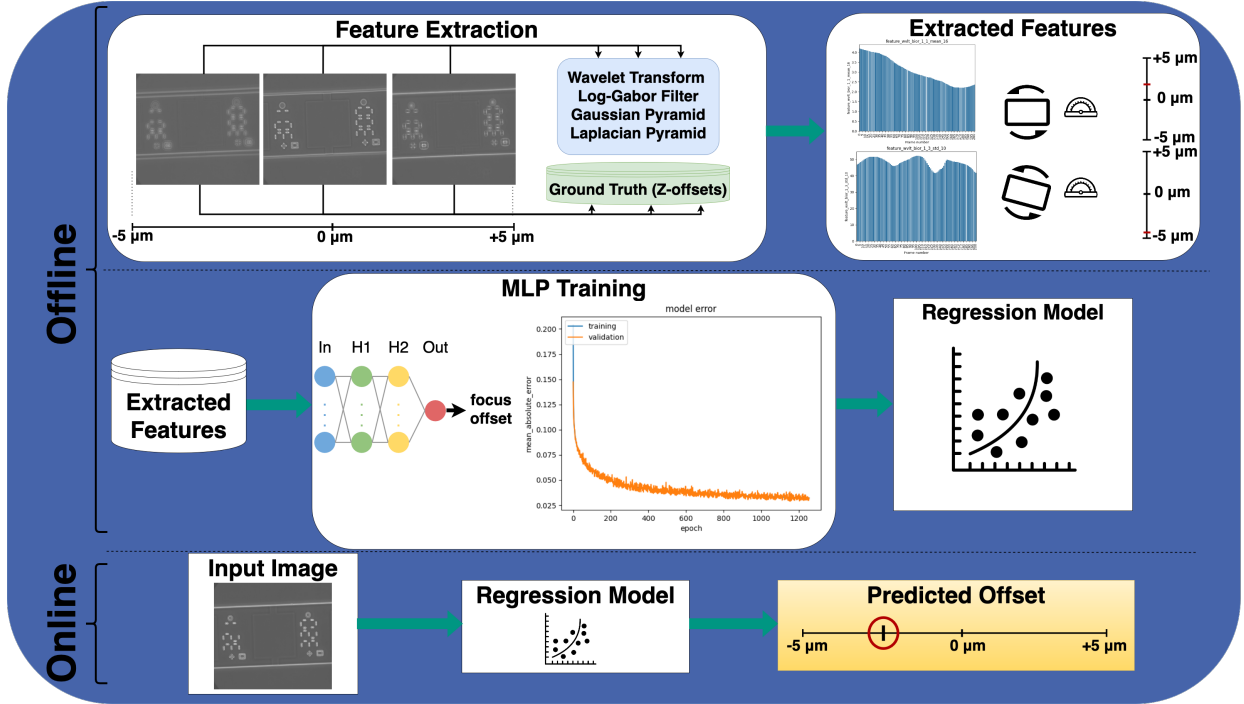


Figure 2: Overview of the MLP-based autofocusing pipeline. The process begins with feature extraction using techniques such as Laplacian and Gaussian pyramids, wavelets, and Log-Gabor filters. These features are augmented with random flips and rotations to improve robustness. A multi-layer perceptron is then trained on the extracted features to predict the focus offset.

4 Experiments

4.1 Autofocusing

4.1.1 Dataset, Metrics and Implementation

The dataset comprises 13,000 high-resolution images (2560×2160 pixels) captured using a Nikon T1 microscope under controlled conditions. These images reflect variations in chamber populations, orientations, and damage levels while maintaining consistent chip design. Data was collected by defining a step size of $0.1 \mu\text{m}$ and acquiring images from each chamber across a focus range of -5 to $+5 \mu\text{m}$, forming a stack where zero represents perfect focus. This approach ensured consistent coverage of the z-axis for all samples and provided a comprehensive dataset for training and evaluation.

All models were implemented using TensorFlow/Keras and trained on an NVIDIA RTX 3090 GPU with 24 GB VRAM, while an Intel Core i9-12900K CPU facilitated preprocessing and evaluation tasks. Model performance was assessed using the MAE by comparing predicted z values with ground truth. The dataset was split into training and a 10% test set for final evaluation (see Sec. 3.1). Therefore, all final MAE metric and error distribution evaluations are based on this test set.

4.1.2 Results

The model is trained using the Adam optimizer, MAE loss, and k-fold cross-validation, with early stopping to prevent overfitting. It achieves a final validation MAE of $0.0262 \mu\text{m}$, ensuring accurate focus predictions. Notably, the MLP does not require advanced hardware and can be trained on standard lab computers within a few hours, making it cost-efficient and accessible.

In real-time operations (with 100 milliseconds of image acquisition time in our context), the model predicts focus adjustments in under 50 milliseconds per image. These predictions feed into a closed-loop control system, enabling the microscope to fine-tune the focus until the optimal point is reached iteratively.

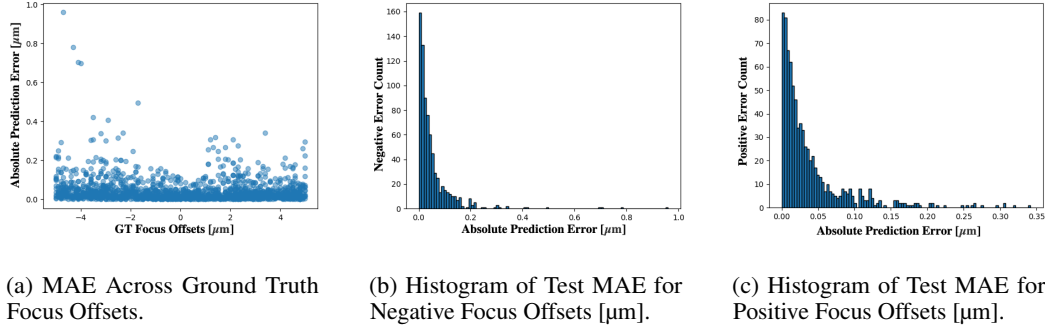


Figure 3: Autofocusing train evaluations.

The model’s performance on the test set was evaluated (see Sec. 3.1) and a range of statistics were collected to understand its error characteristics better. Most errors fall between 0 and 1 μm , which is expected for a focusing system, suggesting that the model is generally precise. The error distribution across different focus offsets (see Fig. 3a) and the associated histograms (see Figs. 3b and 3c) show that the errors are concentrated at lower magnitudes, consistent with the model’s intended behavior. The mean error is 0.0226 μm , with a standard deviation of 0.0216 μm , indicating a relatively tight error range. The 25th, 50th, and 75th percentiles are 0.0073 μm , 0.0154 μm , and 0.0328 μm , respectively, the maximum error is 0.1158 μm .

An interesting observation is that positive and negative focus differences are not identical. Harmful focus errors are predicted to be slightly worse than positive focus errors. This is reflected in the histograms of positive and negative errors (Figures 3b and 3c), suggesting that the model may have a subtle bias toward overestimating the focus offset, leading to slightly larger positive errors. Despite this, the majority of errors still fall within the expected range. Note that the results presented here could change significantly if the chip design were altered. This is because the features extracted from the images and their correlation with the focus offsets would no longer be valid. Any modification to the chip design would require recalibration of the feature extraction process, as the relationship between the features and the focus offset might not hold with the new design.

4.2 Real-Time Image Processing: Segmentation

4.2.1 Dataset, Metrics and Implementation

The benchmark dataset [46] is used to evaluate the methods. The dataset contains images of *Corynebacterium glutamicum* microbes and represents a typical experiment in cell culture. The dataset includes five video sequences of 800 images, each showing the development of the microbes and consists of ground truth instance segmentation mask and tracking annotations. For the context of this work, we use all 4000 images to evaluate the zero-shot segmentation performances. The benchmark was performed on an Ubuntu 22.04 workstation with an Intel Core i9-13900 Central Processing Unit (CPU), a RTX3090 Graphics Processing Unit (GPU) and a 64 GB Random-Access Memory (RAM) chosen as a baseline. To evaluate the segmentation accuracy, the metrics Average Precision (AP) [31], including AP@50 and AP@75 and Panoptic Quality (PQ) [24], comprising Segmentation Quality (SQ) and Recognition Quality (RQ), are calculated for all four methods mentioned in Sec. 2 (see Tab. 2) using TorchMetrics [9]. Since the AP-based metric requires the confidence score for calculation, evaluating this metric for all methods was not possible.

4.2.2 Results

To evaluate the performance of the DL SOTA segmentation methods on microcolonies imaged in a microfluidic live-cell imaging setup, the proposed models (see Sec. 2.2) were evaluated under default settings. The qualitative results are shown in Fig. 4 and the quantitative results are shown in Tab. 2.

CellPose 3 emerged as the best-performing model regarding segmentation quality, achieving the highest PQ of 93.58% and RQ of 99.46%, primarily due to its automatic cell diameter estimation. However, this optimization also resulted in significantly longer inference times (1,115 ms), making it almost 10 times slower than the Distance-based method, achieving comparable qualitative results with a PQ of 93.02%. This trade-off limits the practical applicability of CellPose 3 in time-sensitive workflows, as the marginal improvement in PQ does not justify the substantial increase in computational time.

Omnipose, with a PQ of 93.36% and a fast inference time (271 ms, though slower than the Distance-based method at 121 ms), provided results nearly indistinguishable from CellPose 3 and Distance-based segmentation when evaluated

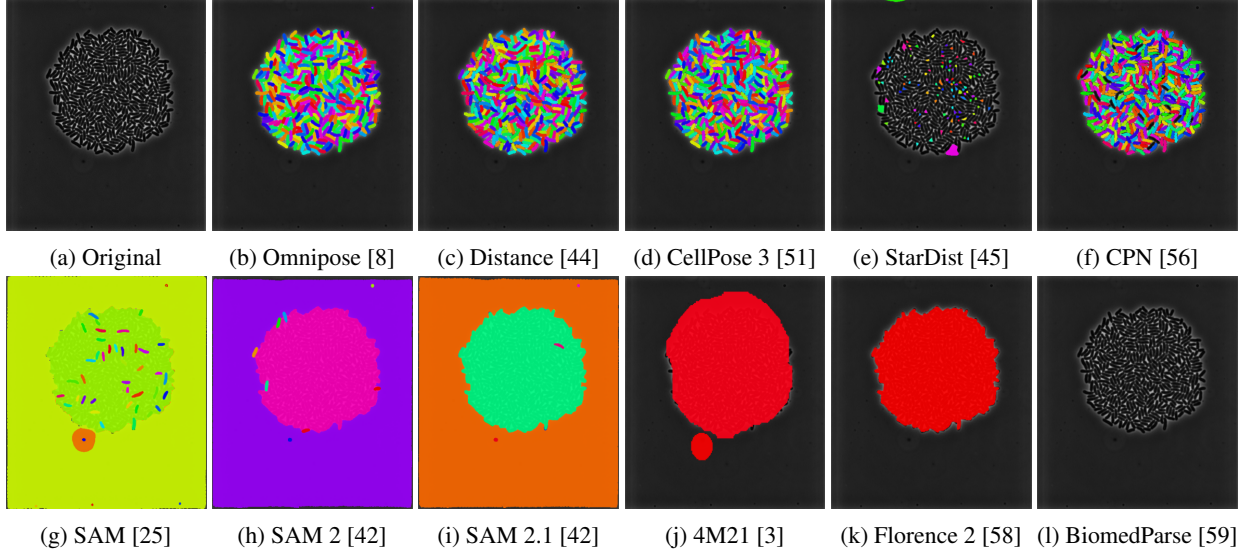


Figure 4: The original image (Fig. 4a) and the zero-shot instance segmentation predictions for [46] (Fig. 4b to Fig. 4l)

Table 2: AP results, PQ results comprising SQ score and RQ score as well as inference times (Inf.) evaluated on the benchmark dataset [46] best in bold. When calculating the metric, falsely detected backgrounds were not removed and evaluated during the AP calculation as false positives. The models were used according to basic configurations for fair comparison. The values in bold are the best across all methods, provided there were results. To ensure a fair comparison, we define inference time as the duration from inputting the image to receiving the model’s prediction as an instance mask with confidence scores. This includes post-processing needed by certain methods, such as converting predicted contours to a pixel-wise mask. The inference time is measured using FP32 precision.

Methods \ Metrics	AP \uparrow [%]	AP@50 \uparrow [%]	AP@75 \uparrow [%]	PQ \uparrow [%]	PQ-SQ \uparrow [%]	PQ-RQ \uparrow [%]	\emptyset Inf. [ms] \downarrow
Omnipose [8]	-	-	-	93.36	93.95	99.35	271
Distance-based [44]	-	-	-	93.02	93.48	99.50	121
Cellpose 3 [51]	-	-	-	93.58	94.07	99.46	1,115
StarDist [45]	0	0	0	36.29	72.87	40.93	7,686
CPN [56]	62.32	95.51	81.70	85.75	87.79	97.63	185
SAM [25]	3.47	4.76	4.70	6.26	84.16	7.36	1,994
SAM 2 [42]	0.27	0.33	0.32	4.85	78.49	6.89	1,566
SAM 2.1 [42]	1.79	2.64	2.45	6.00	76.10	7.98	1,546
4M21 [3]	-	-	-	38.11	47.80	39.86	103,025
Florence 2 [58]	-	-	-	42.00	83.78	43.16	4,294
BiomedParse [59]	0.03	0.07	0	37.63	78.48	41.12	266

visually, reliably detecting all microcolonies, including their number. Both methods proved suitable for practical applications where efficiency and accuracy are critical. Conversely, CPN struggled with detecting densely packed microcolonies, often missing structures in the interior regions of the colonies. The last task-specific model StarDist, optimized for bright objects on dark backgrounds, exhibited significant challenges in detecting dark microcolonies against a dark background, and inverting the contrast introduced additional issues due to background artifacts.

The FMs primarily identified the microcolony as a whole without resolving individual structures. Notably, segmentation accuracy decreased across SAM versions as they performed panoptic segmentation, which led to increased false positives due to the lack of automated background removal in this study. This limitation highlights the challenges of applying these models out-of-the-box. BiomedParse, trained primarily on medical objects such as organs, failed to segment microcolonies sufficiently. While this lack of predictions minimized false positives, the model was ineffective for this application. In contrast, StarDist’s inability to segment microcolonies reliably led to frequent false positives.

Overall, CellPose 3, Omnipose, and Distance-based methods delivered similar high-quality results that were challenging to differentiate visually, with all three reliably identifying microcolonies in terms of count and structure. Given the extended inference time of CellPose 3, Omnipose and Distance-based segmentation present more practical alternatives for real-time applications. This study highlights the importance of selecting models based on experimental requirements, balancing segmentation quality, inference speed, and model robustness.

4.3 Real-Time Data Analysis

The real-time data analysis module contains the event detection and the dashboard.

4.3.1 Event detection

This submodule enables the detection of events in hundreds of parallel experiments. The data and metadata acquired by the other modules are leveraged to detect events at a cultivation chip level, cultivation chamber level or cell level. In our case, based on rules defined by the domain expert, we distinguish between two types of events. The first category includes technical events associated with the devices, such as focus loss or chamber defects. The second category involves biological events that capture microbial behavior, such as growth rates or cell death. Due to the widespread usage of Slack¹ as a communication platform, we built a notifier that sends messages to a Slack channel to inform the user of events that occurred.

4.3.2 Dashboard

The dashboard in this module serves a dual purpose: it updates the experiment's status and includes a microscope control feature, enabling the user to manage the experiment. It currently comprises two primary sections to fulfill these functions: an experiment setup part and an experiment monitoring part.

The experiment setup interface, as highlighted in red in Fig. 5, allows users to configure via dropdown lists the experimental scene, particularly for already documented experiments. The first dropdown is used to select the experiment's cultivation chip. The corresponding heatmap design is prepared and saved for each cultivation chip used. This produces an intuitive chip-based heatmap and improves usability. With the second dropdown, the user chooses the operated microscope. This helps in smoothly gathering necessary feedback and control information. The last dropdown enables the selection of the experiment to be performed. The steps and instructions for frequently performed experiments are saved in a markup language to avoid redundancy in experiment management. In this context, selecting the experiment will execute all documented steps automatically. Once the setup for the experiment is done, the buttons *Start*, *Stop* and *Pause/Resume* can be utilized to manage the experiment.

4.3.3 Results

The experiment monitoring interface has two main analysis focuses. The first focus is the cultivation chip. Fig. 5 shows a heatmap of the cultivation chip with the current state of each cultivation chamber based on a selected option (see radio buttons in the upper left corner). The available options are *cell count*, *cell size*, *event occurrences*, *focus score*. To enhance usability, the heatmap is designed to match the microfluidic chip. The sidebar of Fig. 5 shows metadata relative to the experiment and the user. It also has a button to download experiment results as an Excel file for further analysis.

The second focus is the cultivation chamber. Hovering with the mouse on a chamber in the heatmap displays a box with further data. Clicking on the chamber provides detailed information such as the collected raw images and segmentation masks computed, the state of each key metric (see blue part Fig. 5 and Fig. 6). The sidebar from Fig. 6 provides the history of the selected chamber, along with a filter to show specific messages. The user can receive these messages via a communication platform (currently Slack) app. For analyzing purposes, the user can also visualize the evolution of specific metrics (cell size, cell count, growth rate and focus score) as a function of time. These figures help the domain expert to visualize and analyze the experiments. For example, the segmentation and tracking method can be checked using the 2D+t information from the second row of Fig. 6.

The aim is to deliver a flexible, customizable, and adaptable dashboard suitable for any laboratory. Future work includes essential features for daily experiment monitoring, such as integration with electronic lab notebooks, e.g., eLabFTW [11], which will ease experiment documentation and reporting.

¹<https://slack.com>

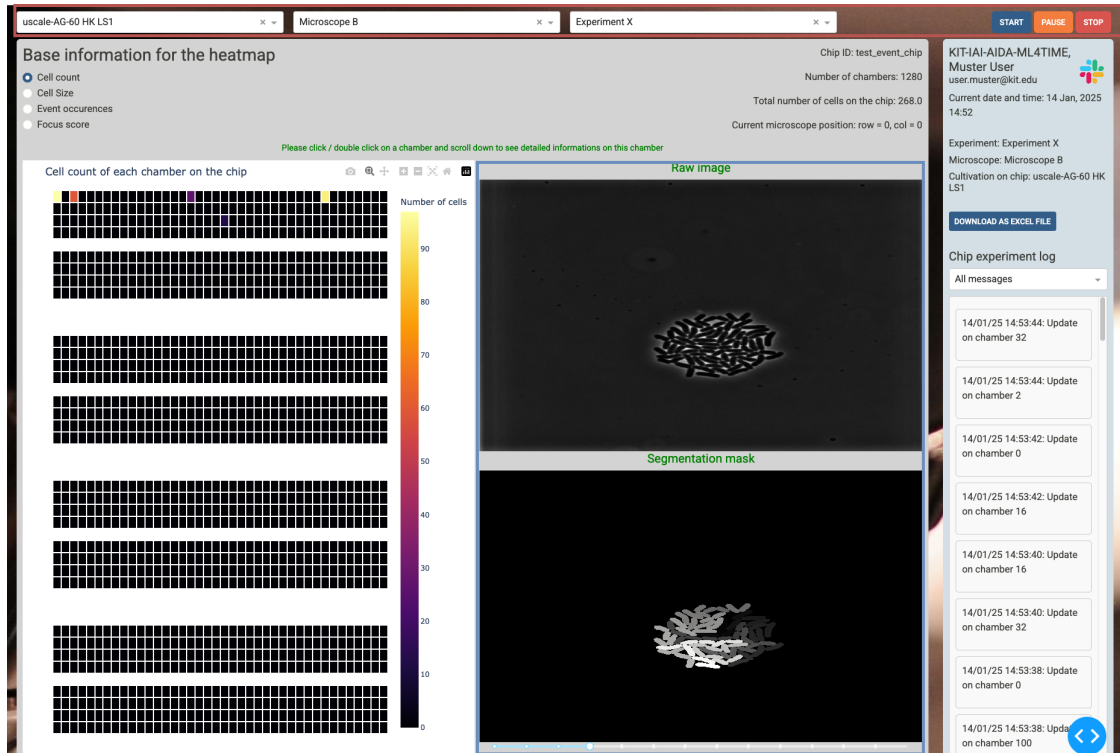


Figure 5: EAP4EMSIG Dashboard (1). User interface for controlling and monitoring an automated microfluidic experiment involving the cultivation of cells on a chip. The interface displays real-time data in live feed for chamber events like cell count, the status of the various chambers, live-image and the progress of the experiment.



Figure 6: EAP4EMSIG Dashboard (2). This view of the user interface shows detailed information for a selected chamber (chamber 0) of the microfluidic chip, including cell number, cell size, growth rate, and focus score. The graphical display allows for real-time monitoring and analysis of cellular parameters during the experiment.

5 Conclusion

This paper provides an in-depth exploration of three key modules within the EAP4EMSIG system. These modules are critical for advancing the platform's real-time imaging and analysis capabilities.

First, we introduce a novel real-time autofocusing module for precise and rapid image acquisition. This module achieves a processing time of under 50 ms while maintaining a MAE of just 0.0226 μm . These results underline its ability to deliver highly accurate and precise image acquisition, essential for effective downstream image analysis and processing tasks. Future research will focus on developing generalized models requiring minimal training data and optimizing speed for live imaging. We plan to update the model as new data becomes available. However, since the interfaces are already in place, we will only need to update the model and architecture without significant changes to the overall framework.

The second focus of this paper is the image processing module. Here, we conducted a comprehensive zero-shot benchmark, evaluating 11 state-of-the-art models across task-specific, domain-specific, and foundation categories. Our analysis revealed that FMs, while robust in other applications, are unsuitable for our task. These models demonstrated low accuracy and unacceptably high processing times, with some exceeding 100 s. In contrast, task-specific models, such as Omnipose and the distance-based method, achieved excellent results with PQ scores exceeding 93%. Furthermore, the distance-based method distinguished itself with a remarkably fast processing time of just 121 ms. Notably, these task-specific methods were trained on bacterial datasets, introducing potential biases compared to domain-specific models. Despite this, the domain-specific model Cellpose 3 also demonstrated promising performance, suggesting it is a strong candidate for further optimization. Future work will explore strategies to accelerate processing times to meet the system's minimum requirement of 100 ms for segmentation. These strategies include converting models to specialized inference formats, such as TensorRT², and transforming models to lower-precision formats like FP16 or Int8.

The final module presented in this paper is the real-time data analysis module. By providing a user-friendly dashboard, biology experts can monitor and analyze experiments as they occur. This tool significantly enhances the ability to oversee and interpret experimental data efficiently by offering real-time control and insights. Future research will aim to improve the accuracy and robustness of the autofocusing module to automate the selection of suitable segmentation methods (see [19, 20, 35, 50]), enhance segmentation speed to meet real-time requirements and expand the functionality of the real-time data analysis module. Additionally, new models are currently under development and will be discussed in greater detail in forthcoming publications.

6 Contributions

The authors have accepted responsibility for the entire content of this manuscript and approved its submission. We describe here the individual contributions: Conceptualization: NF, AJYS, JS, RM; Methodology: NF, AJYS, EY, DK, HS, JS, KN, RM; Software: NF, AJYS, AN, EY, MB, LS, BA, JS; Investigation: NF, AJYS, JS; Resources: JS, KN; Writing – Original Draft: NF, AJYS, MP, MB, ON, EY, JS; Writing – Review & Editing: NF, AJYS, AN, MP, EY, MB, LS, BA, TL, ON, NK, HS, JS, KN, RM; Supervision: DK, HS, KN, RM; Project administration: DK, HS, KN, RM; Funding Acquisition: DK, HS, EY, KN, RM.

7 Acknowledgments

This work was supported by the President's Initiative and Networking Funds of the Helmholtz Association of German Research Centers [Grant EMSIG ZT-I-PF-04-44]. The Helmholtz Association funds this project under the "Helmholtz Imaging Platform", the authors N. Friederich, A. J. Yamachui Sitcheu and R. Mikut under the program "Natural, Artificial and Cognitive Information Processing (NACIP)", the authors N. Friederich and A. J. Yamachui Sitcheu through the graduate school "Helmholtz Information & Data Science School for Health (HIDSS4Health)" and the author Johannes Seiffarth through the graduate school "Helmholtz School for Data Science in Life, Earth and Energy (HDS-LEE)".

References

- [1] *People & Impacts: Report on an American Academy of Microbiology Virtual Colloquium*. American Society for Microbiology, Washington (DC), 2021.

²<https://github.com/NVIDIA/TensorRT>

- [2] C. Allan, J.-M. Burel, J. Moore, C. Blackburn, M. Linkert, S. Loynton, D. MacDonald, W. J. Moore, C. Neves, A. Patterson, et al. OMERO: flexible, model-driven data management for experimental biology. *Nature Methods*, 9(3):245–253, 2012.
- [3] R. Bachmann, O. F. Kar, D. Mizrahi, A. Garjani, M. Gao, D. Griffiths, J. Hu, A. Dehghan, and A. Zamir. 4M-21: An Any-to-Any Vision Model for Tens of Tasks and Modalities. *arXiv 2024*, 2024.
- [4] D. Baddeley, A. E. S. Barentine, Z. Marin, csoeller, actions-user, K. Chung, adrianhollow, D. M. S. Pinto, Mick, Yujin-Bao, and Akalanka. python-microscopy/python-microscopy: Release 23.06.15, 2023.
- [5] Z. Bian, C. Guo, S. Jiang, J. Zhu, R. Wang, P. Song, Z. Zhang, K. Hoshino, and G. Zheng. Autofocusing technologies for whole slide imaging and automated microscopy. *Journal of Biophotonics*, 13(12):e202000227, 2020.
- [6] L. Chiron, M. Le Bec, C. Cordier, S. Pouzet, D. Milunov, A. Banderas, J.-M. Di Meglio, B. Sorre, and P. Hersen. CyberSco. Py an open-source software for event-based, conditional microscopy. *Scientific Reports*, 12(1):11579, 2022.
- [7] A. Croxatto, G. Prod’hom, F. Faverjon, et al. Laboratory automation in clinical bacteriology: what system to choose? *Clinical Microbiology and Infection*, 22(3):217–235, 2016.
- [8] K. J. Cutler, C. Stringer, T. W. Lo, L. Rappez, N. Stroustrup, S. Brook Peterson, P. A. Wiggins, and J. D. Mougous. Omnipose: a high-precision morphology-independent solution for bacterial cell segmentation. *Nature Methods*, 19(11):1438–1448, 2022.
- [9] N. S. Detlefsen, J. Borovec, J. Schock, A. Harsh, T. Koker, L. D. Liello, D. Stancl, C. Quan, M. Grechkin, and W. Falcon. Torchmetrics - measuring reproducibility in pytorch. <https://www.pytorchlightning.ai>, 2022.
- [10] W. R. Drioua, N. Benamrane, and L. Sais. Breast Cancer Detection from Histopathology Images Based on YOLOv5. In *2022 7th International Conference on Frontiers of Signal Processing (ICFSP)*, pages 30–34, 2022.
- [11] eLabFTW Team. elabftw: Open source electronic lab notebook. <https://www.elabftw.net/>, 2025. Accessed: 2025-02-07.
- [12] A. Esteva, K. Chou, S. Yeung, N. Naik, A. Madani, A. Mottaghi, Y. Liu, E. Topol, J. Dean, and R. Socher. Deep learning-enabled medical computer vision. *npj Digital Medicine*, 4(1):5, 2021.
- [13] M. S. Fasihi and W. B. Mikhael. Overview of current biomedical image segmentation methods. In *2016 International Conference on Computational Science and Computational Intelligence (CSCI)*, pages 803–808, 2016.
- [14] Z. R. Fox, S. Fletcher, A. Fraisse, C. Aditya, S. Sosa-Carrillo, J. Petit, S. Gilles, F. Bertaux, J. Ruess, and G. Batt. Enabling reactive microscopy with MicroMator. *Nature Communications*, 13(1):2199, 2022.
- [15] N. Friederich, A. J. Y. Sitcheu, A. Nassal, M. Pesch, E. Yildiz, M. Beichter, L. Scholtes, B. Akbaba, T. Lautenschlager, O. Neumann, et al. EAP4EMSIG–Experiment Automation Pipeline for Event-Driven Microscopy to Smart Microfluidic Single-Cells Analysis. In *Proceedings - 35. Workshop Computational Intelligence: Berlin, 21.-22. November 2024*, volume 24, pages 169–192. KIT Scientific Publishing, 2024.
- [16] N. Friederich and A. Specker. Security Fence Inspection at Airports Using Object Detection. In *Proceedings of the IEEE/CVF Winter Conference on Applications of Computer Vision*, pages 310–319, 2024.
- [17] N. Friederich, A. J. Yamachui Sitcheu, O. Neumann, S. Eroglu-Kayıkçı, R. Prizak, L. Hilbert, and R. Mikut. AI-based automated active learning for discovery of hidden dynamic processes: A use case in light microscopy. In *Proceedings-33. Workshop Computational Intelligence: Berlin, 23.-24. November 2023*, volume 23, page 31. KIT Scientific Publishing, 2023.
- [18] M. Ganesan, R. Mani, S. Sai, G. Kasivelu, M. K. Awasthi, R. Rajagopal, N. I. Wan Azelee, P. K. Selvi, S. W. Chang, and B. Ravindran. Bioremediation by oil degrading marine bacteria: An overview of supplements and pathways in key processes. *Chemosphere*, 303(Pt 1):134956, 2022.
- [19] P. Godau and L. Maier-Hein. Task Fingerprinting for Meta Learning in Biomedical Image Analysis. In *Medical Image Computing and Computer-Assisted Intervention – MICCAI 2021*, pages 436–446. Springer, 2021.
- [20] P. Godau, A. Srivastava, T. Adler, and L. Maier-Hein. Beyond Knowledge Silos: Task Fingerprinting for Democratization of Medical Imaging AI, 2024.
- [21] C. Herrmann, R. S. Bowen, N. Wadhwa, R. Garg, Q. He, J. T. Barron, and R. Zabih. Learning to autofocus. In *Proceedings of the IEEE/CVF Conference on Computer Vision and Pattern Recognition*, pages 2230–2239, 2020.
- [22] I. Holland and J. A. Davies. Automation in the life science research laboratory. *Frontiers in bioengineering and biotechnology*, 8:571777, 2020.

- [23] G. Jocher, A. Chaurasia, A. Stoken, J. Borovec, NanoCode, Y. Kwon, K. Michael, TaoXie, J. Fang, imyhxy, Lorna, z. Yifu), C. Wong, V. Abhiram, D. Montes, Z. Wang, C. Fati, J. Nadar, Laughing, UnglvKitDe, V. Sonck, tkianai, yxNONG, P. Skalski, A. Hogan, D. Nair, M. Strobel, and M. Jain. ultralytics/yolov5: v7.0 - YOLOv5 SOTA Realtime Instance Segmentation. Zenodo, 2022.
- [24] A. Kirillov, K. He, R. Girshick, C. Rother, and P. Dollár. Panoptic segmentation. In *Proceedings of the IEEE/CVF Conference on Computer Vision and Pattern Recognition*, pages 9404–9413, 2019.
- [25] A. Kirillov, E. Mintun, N. Ravi, H. Mao, C. Rolland, L. Gustafson, T. Xiao, S. Whitehead, A. C. Berg, W.-Y. Lo, P. Dollár, and R. Girshick. Segment Anything. *arXiv:2304.02643*, 2023.
- [26] G. Lancini and A. L. Demain. Bacterial pharmaceutical products. In E. Rosenberg, E. F. DeLong, S. Lory, E. Stackebrandt, and F. Thompson, editors, *The Prokaryotes*, pages 257–280. Springer Berlin Heidelberg, Berlin, Heidelberg, 2013.
- [27] J. P. Lewis et al. Fast template matching. In *Vision Interface*, volume 95, pages 15–19. Quebec City, QC, Canada, 1995.
- [28] M. Li, A. Fang, X. Yu, K. Zhang, Z. He, C. Wang, Y. Peng, F. Xiao, T. Yang, W. Zhang, X. Zheng, Q. Zhong, X. Liu, and Q. Yan. Microbially-driven sulfur cycling microbial communities in different mangrove sediments. *Chemosphere*, 273:128597, 2021.
- [29] Q. Li, L. Bai, S. Xue, and L. Chen. Autofocus system for microscope. *Optical Engineering*, 41(6):1289–1294, 2002.
- [30] J. Liao, X. Chen, G. Ding, P. Dong, H. Ye, H. Wang, Y. Zhang, and J. Yao. Deep learning-based single-shot autofocus method for digital microscopy. *Biomedical Optics Express*, 13(1):314–327, 2021.
- [31] T.-Y. Lin, M. Maire, S. Belongie, J. Hays, P. Perona, D. Ramanan, P. Dollár, and C. L. Zitnick. Microsoft COCO: Common Objects in Context. In *Computer Vision—ECCV 2014: 13th European Conference, Zurich, Switzerland, September 6–12, 2014, Proceedings, Part V 13*, pages 740–755. Springer, 2014.
- [32] A. Lou, S. Guan, and M. Loew. CFPNet-M: A Light-Weight Encoder-Decoder Based Network for Multimodal Biomedical Image Real-Time Segmentation. *Computers in Biology and Medicine*, 154:106579, 2023.
- [33] D. Mahecic, W. L. Stepp, C. Zhang, J. Griffié, M. Weigert, and S. Manley. Event-driven acquisition for content-enriched microscopy. *Nature Methods*, 19(10):1262–1267, 2022.
- [34] M. Maška, V. Ulman, P. Delgado-Rodriguez, E. Gómez-de Mariscal, T. Nečasová, F. A. Guerrero Peña, T. I. Ren, E. M. Meyerowitz, T. Scherr, K. Löffler, et al. The cell tracking challenge: 10 years of objective benchmarking. *Nature Methods*, 20(7):1010–1020, 2023.
- [35] M. Molina-Moreno, M. P. Schilling, M. Reischl, and R. Mikut. Automated Style-Aware Selection of Annotated Pre-Training Databases in Biomedical Imaging. In *2023 IEEE 20th International Symposium on Biomedical Imaging (ISBI)*, pages 1–5, 2023.
- [36] J. M. Nduko and S. Taguchi. Microbial production of biodegradable lactate-based polymers and oligomeric building blocks from renewable and waste resources. *Frontiers in Bioengineering and Biotechnology*, 8:618077, 2020.
- [37] N. Otsu et al. A threshold selection method from gray-level histograms. *Automatica*, 11(285-296):23–27, 1975.
- [38] E. Pedone, I. De Cesare, C. G. Zamora-Chimal, D. Haener, L. Postiglione, A. La Regina, B. Shannon, N. J. Savery, C. S. Grierson, M. Di Bernardo, et al. Cheetah: a computational toolkit for cybergenetic control. *ACS Synthetic Biology*, 10(5):979–989, 2021.
- [39] H. Pinkard, N. Stuurman, I. E. Ivanov, N. M. Anthony, W. Ouyang, B. Li, B. Yang, M. A. Tsuchida, B. Chhun, G. Zhang, et al. Pycro-Manager: open-source software for customized and reproducible microscope control. *Nature Methods*, 18(3):226–228, 2021.
- [40] D. M. S. Pinto, M. A. Phillips, N. J. Hall, J. Mateos-Langerak, D. Stoychev, T. S. Pinto, M. J. Booth, I. Davis, and I. M. Dobbie. Python-Microscope – a new open-source Python library for the control of microscopes. *Journal of Cell Science*, 134, 2021.
- [41] A. R Hanna, S. J Shepherd, D. Issadore, and M. J Mitchell. Microfluidic generation of diverse lipid nanoparticle libraries. *Nanomedicine (Lond.)*, 19(6):455–457, Mar. 2024.
- [42] N. Ravi, V. Gabeur, Y.-T. Hu, R. Hu, C. Ryali, T. Ma, H. Khedr, R. Rädle, C. Rolland, L. Gustafson, et al. SAM 2: Segment Anything in Images and Videos. *arXiv preprint arXiv:2408.00714*, 2024.
- [43] C. C. Sachs, K. Ruzaeva, J. Seiffarth, W. Wiechert, B. Berkels, and K. Nöh. CellSium: versatile cell simulator for microcolony ground truth generation. *Bioinformatics Advances*, 2(1):vba053, 2022.

- [44] T. Scherr, K. Löffler, M. Böhlend, and R. Mikut. Cell segmentation and tracking using CNN-based distance predictions and a graph-based matching strategy. *PLoS One*, 15(12):e0243219, 2020.
- [45] U. Schmidt, M. Weigert, C. Broaddus, and G. Myers. Cell Detection with Star-Convex Polygons. In *Medical Image Computing and Computer-Assisted Intervention – MICCAI 2018*, pages 265–273. Springer, 2018.
- [46] J. Seiffarth, L. Blöbaum, R. Paul, N. Friederich, A. J. Yamachui Sitcheu, R. Mikut, H. Scharr, A. Grünberger, and K. Nöh. Tracking one-in-a-million: Large-scale benchmark for microbial single-cell tracking with experiment-aware robustness metrics. In *European Conference on Computer Vision*. Springer, 2024.
- [47] J. Seiffarth, T. Scherr, B. Wollenhaupt, O. Neumann, H. Scharr, D. Kohlheyer, R. Mikut, and K. Nöh. ObiWan-Microbi: OMERO-based integrated workflow for annotating microbes in the cloud. *SoftwareX*, 26:101638, 2024.
- [48] R. Sender, S. Fuchs, and R. Milo. Revised estimates for the number of human and bacteria cells in the body. *PLoS Biology*, 14(8):e1002533, 2016.
- [49] L. Shih. Autofocus survey: A comparison of algorithms. In *Digital Photography III*, volume 6502, pages 90–100. SPIE, 2007.
- [50] A. Y. Sitcheu, N. Friederich, S. Baeuerle, O. Neumann, M. Reischl, and R. Mikut. MLOps for Scarce Image Data: A Use Case in Microscopic Image Analysis. In *Proceedings-33. Workshop Computational Intelligence: Berlin, 23.-24. November 2023*, volume 23, page 169. KIT Scientific Publishing, 2023.
- [51] C. Stringer and M. Pachitariu. Cellpose3: one-click image restoration for improved cellular segmentation. *Nature Methods*, Feb 2025.
- [52] C. Stringer, T. Wang, M. Michaelos, and M. Pachitariu. Cellpose: a generalist algorithm for cellular segmentation. *Nature Methods*, 18(1):100–106, 2021.
- [53] B. Sun, W. Zhang, C. Xing, and Y. Li. Underwater moving target detection and tracking based on enhanced you only look once and deep simple online and realtime tracking strategy. *Engineering Applications of Artificial Intelligence*, 143:109982, 2025.
- [54] Y. Sun, S. Duthaler, and B. J. Nelson. Autofocusing in computer microscopy: selecting the optimal focus algorithm. *Microscopy Research and Technique*, 65(3):139–149, 2004.
- [55] D. M. Sylvia, J. J. Fuhrmann, P. G. Hartel, and D. A. Zuberer. *Principles and applications of soil microbiology*. Pearson, 2005.
- [56] E. Upschulte, S. Harmeling, K. Amunts, and T. Dickscheid. Contour proposal networks for biomedical instance segmentation. *Medical Image Analysis*, 77:102371, 2022.
- [57] R. Wang, T. Lei, R. Cui, B. Zhang, H. Meng, and A. K. Nandi. Medical image segmentation using deep learning: A survey. *IET Image Processing*, 16(5):1243–1267, 2022.
- [58] B. Xiao, H. Wu, W. Xu, X. Dai, H. Hu, Y. Lu, M. Zeng, C. Liu, and L. Yuan. Florence-2: Advancing a unified representation for a variety of vision tasks. In *Proceedings of the IEEE/CVF Conference on Computer Vision and Pattern Recognition*, pages 4818–4829, 2024.
- [59] T. Zhao, Y. Gu, J. Yang, N. Usuyama, H. H. Lee, S. Kiblawi, T. Naumann, J. Gao, A. Crabtree, J. Abel, C. Moungh-Wen, B. Piening, C. Bifulco, M. Wei, H. Poon, and S. Wang. A foundation model for joint segmentation, detection and recognition of biomedical objects across nine modalities. *Nature Methods*, 22(1):166–176, Jan 2025.